

Hydrogenated graphene nanoribbons for spintronicsD. Soriano,^{1,2} F. Muñoz-Rojas,^{1,3} J. Fernández-Rossier,¹ and J. J. Palacios^{1,4}¹*Departamento de Física Aplicada, Universidad de Alicante, San Vicente del Raspeig, Alicante 03690, Spain*²*Instituto de Ciencia de Materiales de Madrid (CSIC), Cantoblanco, 28049 Madrid, Spain*³*Department of Physics, Korea Advanced Institute of Science and Technology, Daejeon 305-701, Korea*⁴*Departamento de Física de la Materia Condensada, Universidad Autónoma de Madrid, Cantoblanco, Madrid 28049, Spain*

(Received 7 January 2010; published 5 April 2010)

We show how hydrogenation of graphene nanoribbons at small concentrations can open venues toward carbon-based spintronics applications regardless of any specific edge termination or passivation of the nanoribbons. Density-functional theory calculations show that an adsorbed H atom induces a spin density on the surrounding π orbitals whose symmetry and degree of localization depends on the distance to the edges of the nanoribbon. As expected for graphene-based systems, these induced magnetic moments interact ferromagnetically or antiferromagnetically depending on the relative adsorption graphene sublattice, but the magnitude of the interactions are found to strongly vary with the position of the H atoms relative to the edges. We also calculate, with the help of the Hubbard model, the transport properties of hydrogenated armchair semiconducting graphene nanoribbons in the diluted regime and show how the exchange coupling between H atoms can be exploited in the design of novel magnetoresistive devices.

DOI: [10.1103/PhysRevB.81.165409](https://doi.org/10.1103/PhysRevB.81.165409)

PACS number(s): 73.20.-r, 72.80.Vp, 85.75.-d

I. INTRODUCTION

There is a widespread consensus on the large potential of graphene for electronic applications.^{1,2} Theoretically, graphene also holds promise for a vast range of applications in spintronics, although clear evidence of magnetic graphene is, however, elusive to date. In a broad sense, two factors may account for this elusiveness. First, the fact that hydrocarbons of high spin are known to be highly reactive and, unless fabricated or synthesized under very clean and controlled conditions, they will likely bind surrounding species with the concomitant disappearance of magnetism.³ A second reason relates to the fact that the ground state of graphene is near an interaction-driven phase transition into an insulating antiferromagnetic (AF) state.⁴ This underlying antiferromagnetic correlations prevent the magnetic moments, even if they develop, from ordering ferromagnetically and preclude the possibility of observing hysteresis in standard magnetic measurements. Notwithstanding, a few reports of magnetic graphite⁵ and graphene⁶ can be found in recent literature.

Most of recent theoretical ideas for graphene-based spintronics applications are rooted on the magnetic properties of nanoribbons⁷⁻¹¹ or nanographenes¹²⁻¹⁵ with zigzag edges. All these proposals assume a very particular edge hydrogenation where H atoms passivate the σ dangling bonds, leaving all the π orbitals unsaturated and carrying the magnetic moments. However, this is just one out of many possible edge realizations which range from H-free self-passivation¹⁶ to full H passivation.¹⁷ According to the work of Wassmann *et al.*,¹⁷ relatively low H concentrations at room temperature suffice to completely passivate the edges, including the edge π orbitals responsible for the magnetic order. The self-passivated or reconstructed zigzag edges¹⁶ are, in fact, among the least energetically favorable of all, although, interestingly, have been recently observed by transmission electron microscopy.¹⁸

In the light of the present controversy on the actual possibilities of ever encounter zigzag magnetic edges, we pro-

pose in this work an alternative to edge-related spintronics in which to exploit the recently shown controlled hydrogenation of graphene.¹⁹ The key factor here is that adsorption of atomic H in the bulk of graphene is accompanied by the appearance of a magnetic moment of $1\mu_B$ localized on the π orbitals surrounding each H atom.²⁰ These magnetic moments interact with one another ferromagnetically or antiferromagnetically, depending on whether their respective adsorption sublattices (usually labeled A and B) are the same or not.²⁰⁻²² Statistically speaking, a sublattice compensated H coverage is expected unless adsorption on one sublattice is privileged, e.g., by the substrate. To date, however, there is no evidence that such an uncompensated coverage can be achieved. In the more likely compensated case an overall antiferromagnetic alignment with a total spin $S=0$ is thus energetically favored over a ferromagnetic (F) one with $S > 0$. As a proof of principle and since we are interested in the diluted regime, we consider in this work the fundamental problem of two H atoms. These are covalently bonded to the surface of a semiconducting armchair graphene nanoribbon (AGNR) on different sublattices [see Fig. 1(a)]. Here the σ bonds of the edges are fully passivated with H so that they are irrelevant at low energies.

As shown in Sec. III, after a brief introduction to the theoretical basics presented in Sec. II, the magnetic-field driven F state, where the H-induced magnetic moments are aligned by the field [as shown in Fig. 2(b)], can present a different resistance from that of the natural AF zero-field state [as that in Fig. 2(a)]. Two different cases are discussed: infinite semiconducting AGNR's and finite ones connected to conductive graphene [see schematic picture in Fig. 1(d)]. The differences in conductance between the F and the AF states can be substantial and translate into a magnetoresistive response as large as 100% for distances between the H atoms of the order of few nanometers. Practical implications of these results are discussed in Sec. IV and a brief summary is presented in Sec. V

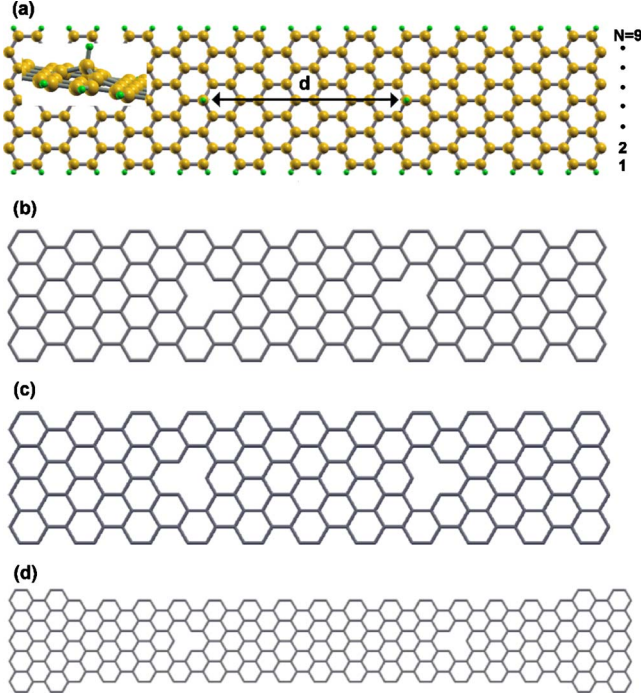


FIG. 1. (Color online) (a) Armchair graphene nanoribbon of width N (where N is the number of dimer lines) with two H atoms adsorbed in the middle of the ribbon at a distance d from each other. The inset shows a detail of the adsorption geometry. (b) Pictorial representation of the one-orbital tight-binding model where the presence of H atoms is simulated by removing sites in a head-to-head configuration. (c) Same as in (b) but for the opposite ordering (tail to tail). (d) Same as in (b) but for a finite semiconducting AGNR connected to metallic nanoribbons at the edges.

II. COMPUTATIONAL DETAILS

For the calculation of the electronic structure of hydrogenated AGNR's we use both *ab initio* techniques within the local spin-density approximation (LSDA), aided by the CRYSTAL03 package,²³ and a one-orbital (π) first-neighbor tight-binding model where the electronic repulsion is treated by means of a Hubbard-type interaction U in the mean-field approximation,

$$\hat{H} = \sum_{i,j} t \hat{c}_i^\dagger \hat{c}_j + U \sum_i (\hat{n}_{i\uparrow} \langle \hat{n}_{i\downarrow} \rangle + \hat{n}_{i\downarrow} \langle \hat{n}_{i\uparrow} \rangle) - U \sum_i \langle \hat{n}_{i\downarrow} \rangle \langle \hat{n}_{i\uparrow} \rangle. \quad (1)$$

The first term represents the kinetic energy with first neighbors hopping t between π orbitals. The remaining terms account for the electronic interactions where $\hat{n}_{i\eta} = \hat{c}_{i\eta}^\dagger \hat{c}_{i\eta}$ are the number operators associated to each π orbital with spin η . These two different levels of approximation to the electronic structure have been shown to yield similar results for nanoribbons²⁴ and nanographenes¹³ where a full passivation by H of the σ bonds is assumed.

The bulk adsorption geometry of a H atom has been obtained by relaxing the C atom bonded to the H and the nearest C atoms until the characteristic sp^3 hybridization is obtained [see inset in Fig. 1(a)]. The bonding between a H atom

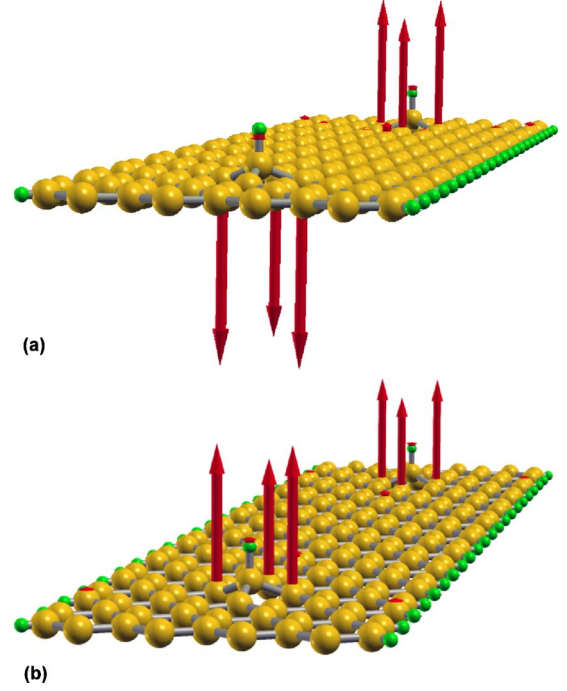


FIG. 2. (Color online) (a) Pictorial view of the antiferromagnetic state and (b) the magnetic-field driven ferromagnetic state where the magnetic moments localized around two hydrogen atoms are depicted by red arrows (the orientation of the arrows with respect to the graphene plane is arbitrary since spin-orbit coupling is neglected here).

and a C atom results in the effective removal of the π orbital from the low-energy sector so that the H adsorption is simulated by simply removing a site in the one-orbital mean-field Hubbard model [see Figs. 1(b)–1(d)]. Our results, as shown below, provide further support to the use of the Hubbard model in graphene systems, as an alternative to the computationally more demanding LSDA and extend the range of applicability of Lieb's theorem²⁵ to a wider set of situations.

To calculate the transport properties we use the standard Green's-function partitioning method as implemented, e.g., in the quantum transport package ALACANT.²⁶ To this purpose, the infinite system is divided into three parts, namely, a central region (C), containing the H atoms, which is connected to the right (R) and left (L) semi-infinite clean leads. The Hamiltonian matrix describing the whole system is then given by

$$H = H_C + H_R + H_L + V_{LC} + V_{RC}, \quad (2)$$

where H_C , H_L , and H_R are the Hamiltonian matrices of the central region, the left and the right lead, respectively. V_{LC} and V_{RC} represent the coupling between the central region and the leads. In general, the nonorthogonality of the basis set must be taken into account when writing the Green's function of the central region,

$$G_C(E) = [ES_C - H_C - \Sigma_L(E) - \Sigma_R(E)]^{-1}. \quad (3)$$

The self-energies of the left (Σ_L) and right (Σ_R) leads account for the influence of these on the electronic structure of

the central part and S_C is the overlap matrix in this region. For the calculation of the conductance we use the Landauer formula, $G(E) = \frac{e^2}{h} T(E)$. The transmission function T can, in turn, be obtained from the expression,

$$T(E) = \sum_{\eta} \text{Tr}[G_C^{\dagger}(E)\Gamma_R(E)G_C(E)\Gamma_L(E)]_{\eta}, \quad (4)$$

with $\Gamma_{R(L)} = i(\Sigma_{R(L)} - \Sigma_{R(L)}^{\dagger})$. Notice that since we are interested in collinear magnetic solutions, all the matrices carry the spin index η , which we have not made explicit in previous equations. All the terms in Eq. (2) must be obtained self-consistently either from a periodic boundary condition calculation, e.g., using CRYSTAL03 in the case of the LSDA calculations, or following the methodology in Ref. 9 in the case of the Hubbard model. The Fermi energy is set to zero and, in both cases, global charge neutrality in all regions is imposed by shifting the onsite energies as necessary.

III. RESULTS

A. Energetics

We first examine the energetics of the F ($S=1$) and AF ($S=0$) states as a function of the mutual distance d between H atoms. We first choose a semiconducting AGNR of width $N=9$, where N is the number of dimer lines across the ribbon, and restrict ourselves to the case of H atoms placed on different sublattices [see Fig. 1(a)]. The reason for this choice is threefold. The AB (or BA) configurations are always energetically preferred to the AA or BB configurations for similar distances between H atoms.²² Second, and most importantly for the purpose of this work, the magnetic state of the AB (or BA) configuration can be tuned by a magnetic field. Furthermore, as briefly mentioned in Sec. I, even if energetic considerations are left aside, the AB (or BA) configuration represents the simplest case of a random ensemble of H atoms which, in average, will equally populate the two graphene sublattices.

In Fig. 3(a) we plot the LSDA total energy for H atoms in the middle of the AGNR as a function of d . The $S=0$ state is always the ground state. This implies antiferromagnetic coupling, except at short distances for which the local magnetization, quantified through $\Sigma = \sqrt{\sum_i \langle m_i \rangle^2}$, vanishes altogether [see Fig. 4(c)]. The quenching of the magnetization is easily understood in terms of the formation of a spin singlet.²⁷ At the minimum distance for which $\Sigma \neq 0$, the energy difference presents a maximum and decays exponentially for larger d [see inset in Fig. 3(a)]. As $d \rightarrow \infty$ the spin clouds do not interact anymore and both F and AF solutions tend to have the same energy. In summary, for any distance between H atoms the ground state presents $S=0$, following Lieb's theorem,²⁵ but the overall spin texture strongly depends on their mutual distance. We note that it also depends on the ordering (AB or BA) of the H atoms. Whereas in bulk the spin cloud associated to the H atom would be invariant under rotations of 120° , in a nanoribbon there is a preferential direction along the ribbon axis which is different for H atoms located on A and B sublattices [see Figs. 1(b) and 1(c)]. We refer to the preferential direction as the head and the tail to

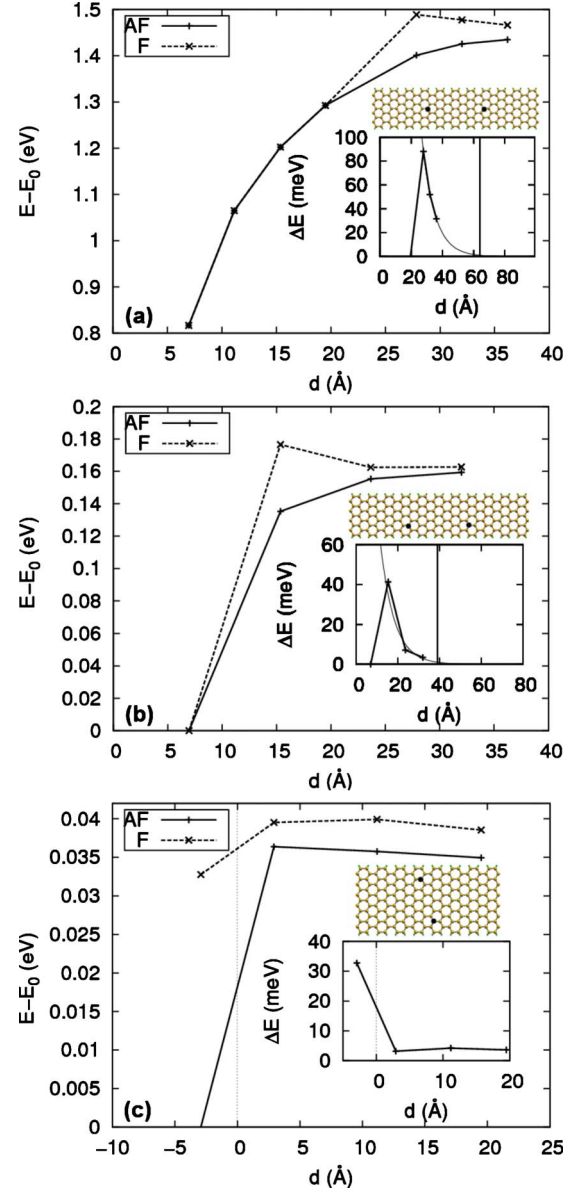


FIG. 3. (Color online) (a) Total energy referred to E_0 [lowest energy in case (b)] as a function of the distance between H atoms for the ferromagnetic (dashed) and the antiferromagnetic (solid) state when placed in the middle of the ribbon. Upper inset: picture of a nanoribbon with two H atoms. Lower inset: energy difference between both states and extrapolation to large distances (solid line). The vertical line in the inset denotes the distance above which the energy difference becomes less than 1 meV. (b) Same as in (a) but for both H atoms near the same edge. (c) Same as in (a) but for H atoms placed on opposite edges. Here the width of the ribbon is larger ($N=13$) and E_0 is the minimum energy among all the AF solutions.

the opposite one. Thus, a head-to-head coupling (AB) is expected to be much stronger than a tail-to-tail coupling (BA). The magnetization clouds are shown for an AB (or head to head) case in Figs. 4(a) and 4(b). It is easy to appreciate the strong directionality just alluded to. As a consequence, when reversing the ordering of the H atoms to a BA (or tail-to-tail) configuration [see Fig. 1(c)], these do not couple magneti-

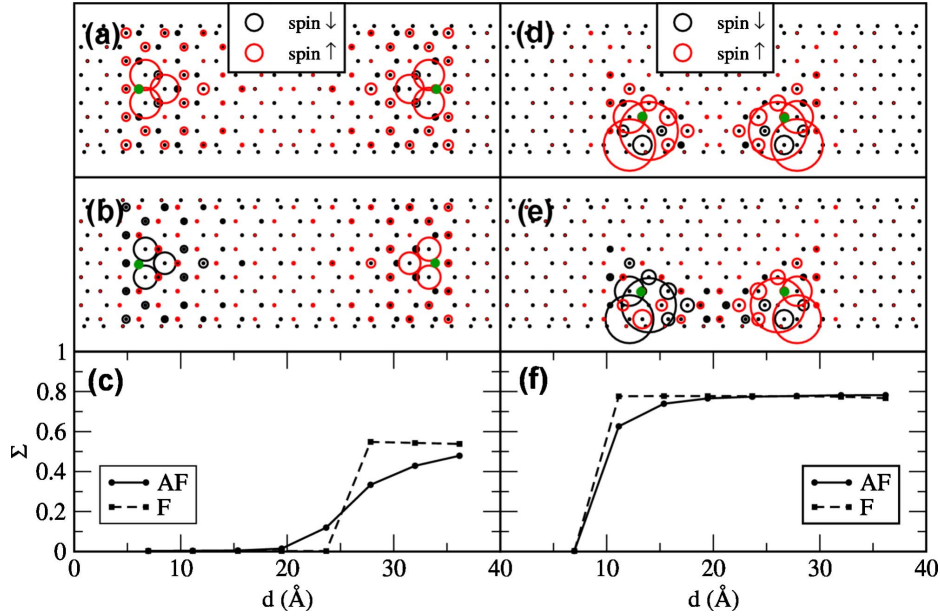


FIG. 4. (Color online) Magnetic moments (whose magnitude is represented by the size of the circles) on individual C atoms when the H atoms are placed head to head in the middle of an $N=9$ armchair graphene nanoribbon at a distance $d=32.0$ Å: [(a) ferromagnetic state and (b) antiferromagnetic state] and at a distance $d=15.4$ Å: close to the edge [(d) ferromagnetic state and (e) antiferromagnetic state]. Panels (c) and (f) show the magnetization (see definition of Σ in text) as a function of the distance between H atoms.

cally at any distance, except when in very close proximity for which $\Sigma=0$. All these results are similar to the ones reported using the one-orbital mean-field Hubbard model.²⁷

In Fig. 3(b) we present the LSDA total energy of the F and AF states when the H atoms are placed near one of the edges. Again the ground state is the AF state for any distance. The proximity to the edge decreases the localization length of the spin texture, increasing Σ [see Figs. 4(d) and 4(e)], and thereby, decreasing the critical distance below which the magnetization disappears [see Fig. 4(f)]. The perturbation of the edge modifies the spin texture around each atom and, contrary to the previous case, when reversing the ordering to a tail-to-tail configuration, the H atoms couple magnetically in a finite range of distances (see below). All energies, including those depicted in Fig. 3(a), are referred to E_0 , the lowest-energy solution for H atoms close to the edge, corresponding to the smallest distance. Note that for the same distance between H atoms the total energy is always smaller when these are closer to the edge, which reflects that the binding energy is higher there by approximately 1 eV.²⁸

Finally we present in Fig. 3(c) the case where the H atoms are placed on opposite edges for an $N=13$ semiconducting AGNR. Placing the atoms on different edges allows us now to explore the energetics of different magnetic coupling orientations (tail to tail for $d>0$ and head to head for $d<0$) at a reasonable computational cost (d is now the longitudinal distance between H atoms). As expected, due to the strong anisotropy of the spin texture, the magnetic coupling strongly depends on the ordering of the atoms and not only on their mutual distance. While for $d<0$ the energy difference between the AF and F states is large, for $d>0$ this difference decreases substantially and does not depend too much on d for the values considered. This asymmetry is easily understood since for $d>0$ ($d<0$) the spin textures ap-

proximately couple in a tail-to-tail (head-to-head) manner. As shown below, this may have important experimental consequences.

B. Magnetoresistance

We now turn our discussion to the implications these results may have on the electrical transport. Under the influence of a magnetic field, the hydrogenated AGNR behaves like a diluted paramagnetic semiconductor²⁹ for small concentrations of H. At large concentrations, when the spin density is zero everywhere, the influence of the field can only give rise to a minor diamagnetic response. At intermediate concentrations, where the magnetization clouds induced by the H atoms interact with each other, one can switch from the AF to the F state by applying a sufficiently strong magnetic field. In analogy with the H_2 molecule, where switching from the singlet to the triplet state modifies the orbital part of the wave function, here the electronic structure will be indirectly affected by the field even if its direct influence on the orbital wave function is neglected. This change reflects in the spin-resolved conductance as shown in Figs. 5(a) and 5(b) for $d=32$ Å: (the dashed line represents the conductance of the clean AGNR). The different total transmission for the F and AF solutions, resulting from adding the two spin channels, results in a positive magnetoresistance (MR), defined as $MR = G_F - G_{AF} / G_F + G_{AF}$, at energies near the bottom and top of the conduction and valence bands, respectively [see Fig. 5(c)]. Similar results are obtained (not shown) for different intermediate distances between H atoms. The right panels in Fig. 5 show the results obtained from the one-orbital mean-field Hubbard model for $U=t=3$ eV. Apart from the recovery of the particle-hole symmetry, the results are remarkably

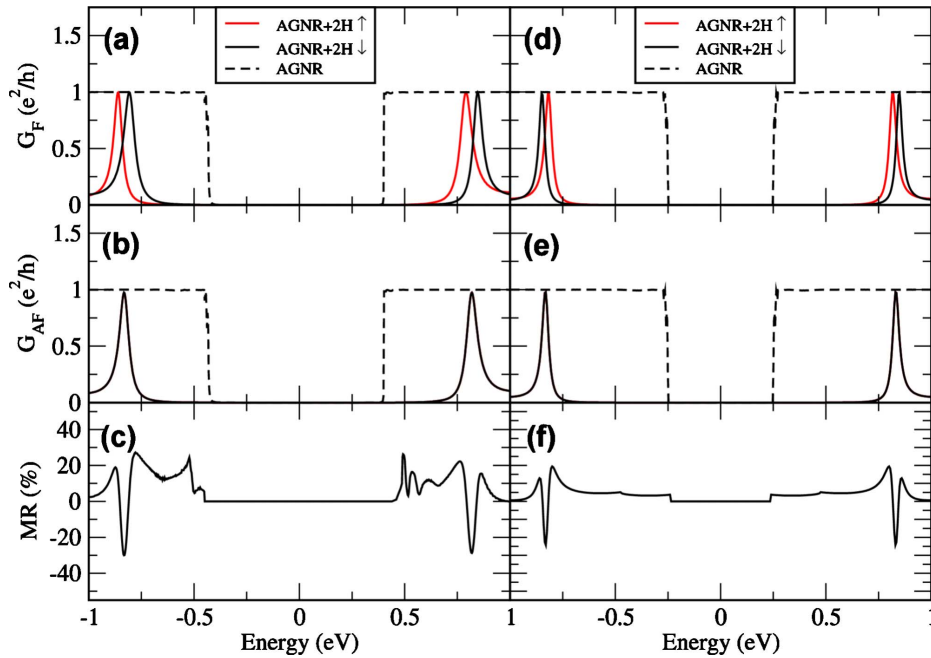


FIG. 5. (Color online) Spin-resolved transmission as a function of energy for the ferromagnetic state of an armchair graphene nanoribbon of width $N=9$ with two H atoms adsorbed in the middle at a mutual distance $d=32 \text{ \AA}$: calculated in the (a) local spin-density approximation and (d) with a one-orbital mean-field Hubbard model. (b) and (e) panels show the same but for the antiferromagnetic state. The resulting magnetoresistance in both approximations is shown in (c) and (f).

similar, validating the use of the latter model for transport calculations in hydrogenated graphene.

One should note, however, that since the chemical potential lies in the middle of the gap, the energy ranges at which MR could manifest itself are not relevant in linear-response transport for infinite AGNR's. A finite bias calculation may reveal the MR obtained at those energies but this is a non-trivial task beyond the scope of this work. The application of a gate voltage is not a practical alternative either since it implies a deviation from charge neutrality which would fill up or empty the localized states hosting the unpaired spins and kill the magnetization. Instead, we propose to explore the possibility of MR at zero bias by considering *finite* AGNR's connected at the ends to conductive graphene. This is done in our calculations by considering a metallic AGNR with a narrower section in the middle of appropriate width [see Fig. 1(d)]. (Note that in the one-orbital mean-field Hubbard approximation AGNR's of width $N=3m-1$, where m is an integer, are metallic, being semiconducting otherwise.) In what follows and in the light of the previous results, we restrict ourselves to the one-orbital mean-field Hubbard model.

In our proposed AGNR heterostructure the difference in the zero-bias tunnel conductance between the F and AF states is now responsible for the appearance of *tunneling* MR (TMR), as shown in Fig. 6. Notice that unlike conventional TMR, where the magnetic elements are in the electrodes, in our proposal magnetism is in the barrier. Panels (a) and (b) in Fig. 6 correspond to H atoms placed in the middle of a semiconducting AGNR of length $L=73.7 \text{ \AA}$: and width $N=9$ and $N=15$, respectively. Both cases refer to head-to-head configurations. The obtained TMR changes sign with d but it is

always negligibly small. On the contrary, when placed near the edge [Fig. 6(c)], the TMR is positive and reaches much larger values. This result is for an $N=9, L=57.0 \text{ \AA}$: AGNR. When the H atoms are now placed in a tail-to-tail configuration near the edge for the same AGNR, the TMR becomes negative and reaches values of up to 100% [see Fig. 6(d)]. As a final example we show in Fig. 7 the TMR for the case

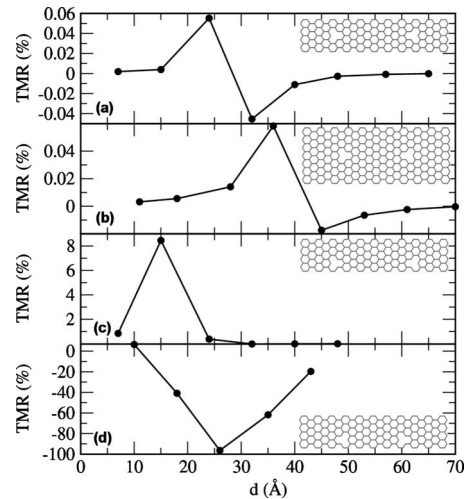


FIG. 6. Tunneling magnetoresistance for four different atomic H configurations obtained with the Hubbard model. Two H atoms in a head-to-head configuration located in the middle of an armchair graphene nanoribbon of length $L=73.7 \text{ \AA}$: with a width of (a) $N=9$ and (b) $N=15$, and two H atoms located near one edge (c) in a head-to-head and (d) in a tail-to-tail configuration for a ribbon width of $N=9$ and length of $L=57.0 \text{ \AA}$.

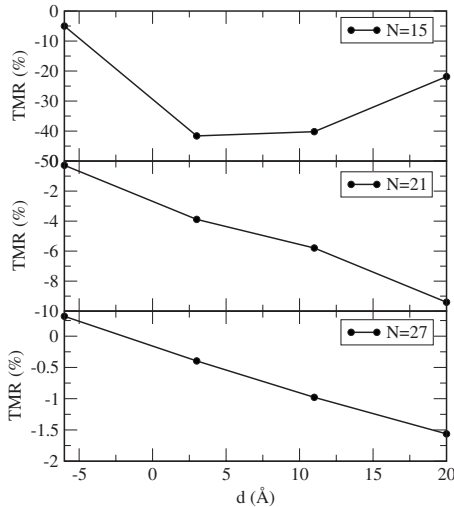


FIG. 7. Tunneling magnetoresistance (obtained with the Hubbard model) as a function of the longitudinal distance between H atoms for three different armchair graphene nanoribbon widths. The H atoms are located on opposite edges of the ribbon.

where the H atoms are placed on the opposite edges of an $L=57.0$ Å: AGNR for three different widths. Large (and negative) values are also obtained for the tail-to-tail configurations in the range of distances explored. As can be appreciated, the TMR logically decreases with the ribbon width.

IV. PRACTICAL CONSIDERATIONS

A critical assessment of the practical consequences of the results presented is due at this point: (1) first, the TMR results presented above have been obtained for a particular type of AGNR heterostructure and rely on the existence of metallic AGNR's. Calculations where the relaxation of the atomic structure on the edges is considered reveal that a gap always opens even for the nominally metallic armchair nanoribbons,³⁰ compromising the applicability of these nanoribbons as electrodes. Graphene-based metallic leads, however, can be found in recent literature. For instance, zigzag graphene nanoribbons with passivated edges are metallic.¹⁷ The physics described in this work does not rely on the edge termination of the nanoribbons and could be reproduced in fully passivated zigzag nanoribbons as well. Another alternative can be based on using partially unzipped metallic carbon nanotubes,³¹ as suggested in Ref. 32. A third possibility consists in gating selectively a semiconducting AGNR as previously done for nanotubes.³³

(2) From the LSDA calculations we note that the energy difference between the F and AF states, or exchange coupling energy, can be as large as tens of millielectron volts for short distances, particularly for head-to-head configurations. However, as far as magnetoresistive properties is concerned, exchange coupling energies above 1 meV are of no practical use since the Zeeman energy gain per spin in a magnetic field B is $0.067g\mu_B B$ meV T⁻¹ and fields higher than 10 T

are hardly accessible in the laboratory. The AF-F transition is therefore practically forbidden below $d \approx 65$ Å: and $d \approx 40$ Å: in the examples shown in Figs. 3(a) and 3(b), respectively. At larger distances the fields necessary to induce the AF-F transition can be as small as needed but also is the associated MR as shown in Figs. 6(a) and 6(c). This is not a problem, however, when the H atoms are coupled tail to tail as, e.g., in the cases where they are located on opposite edges. There, as shown in Fig. 7, a TMR as high as $\approx 50\%$ can be obtained at reasonably small exchange coupling energies [see inset in Fig. 3(c)].

(3) The third caveat relates to the stability of the atomic configurations. Given the tendency for H atoms to form lowest-energy nonmagnetic aggregates,²⁸ the existence of magnetically active dilute ensembles of adsorbed H atoms requires certain conditions. For instance, working at reasonable low temperatures prevents H atoms from diffusing after adsorption.³⁴ Another possibility is one intrinsic to AGNR's: the binding energy is larger for H atoms close to the edge than in the bulk of the nanoribbon. Related to this is the fact that the mobility of H decreases significantly near the edge, reducing the possibility of formation of lowest-energy nonmagnetic aggregates near the edge.²⁸ As we have shown, it is precisely the hydrogenation near the edge that favors the appearance of sizable MR and thus an actual experimental verification.

V. SUMMARY

In summary, we have shown, as a proof of principle, that hydrogenated AGNR's at small concentrations can exhibit magnetoresistive properties without invoking purely edge-related physics. Our results, which are deeply rooted in Lieb's theorem, provide further evidence for the wide applicability of this theorem beyond the bipartite lattice Hubbard model for which was demonstrated. We have also shown that hydrogenation near the edge presents advantages with respect to bulk hydrogenation both from energetic and electronic standpoints. This aspect, specific to nanoribbons, might favor the use of these ones for spintronics applications, as opposed to using large flakes of graphene. Although our conclusions are based on the simplest case of two H atoms, nothing seems to prevent magnetoresistance from occurring for ensembles of many H atoms. The cases exhibiting negative magnetoresistance show larger absolute values than the ones exhibiting positive magnetoresistance. This points toward a generic negative MR for random hydrogenation. This, however, still needs to be supported by a more extensive statistical analysis which is beyond the scope of this work.

ACKNOWLEDGMENTS

This work has been financially supported by MICINN of Spain (Grants No. MAT07-67845 and CONSOLIDER No. CSD2007-00010). D.S. acknowledges financial support from Consejo Superior de Investigaciones Científicas (CSIC).

- ¹A. K. Geim and A. H. MacDonald, *Phys. Today* **60**(8), 35 (2007).
- ²A. H. Castro Neto, F. Guinea, N. M. R. Peres, K. S. Novoselov, and A. K. Geim, *Rev. Mod. Phys.* **81**, 109 (2009).
- ³*Carbon Based Magnetism: An Overview of the Magnetism of Metal Free Carbon-based Compounds and Materials*, edited by T. Makarova and F. Palacio (Elsevier Science & Technology, 2006).
- ⁴S. Sorella and E. Tosatti, *Europhys. Lett.* **19**, 699 (1992).
- ⁵P. Esquinazi, D. Spemann, R. Höhne, A. Setzer, K. H. Han, and T. Butz, *Phys. Rev. Lett.* **91**, 227201 (2003).
- ⁶Y. Wang, Y. Huang, Y. Song, X. Zhang, Y. Ma, J. Liang, and Y. Chen, *Nano Lett.* **9**, 220 (2009).
- ⁷M. Fujita, K. Wakabayashi, K. Nakada, and K. Kusakabe, *J. Phys. Soc. Jpn.* **65**, 1920 (1996).
- ⁸Y.-W. Son, M. L. Cohen, and S. G. Louie, *Nature (London)* **444**, 347 (2006).
- ⁹F. Muñoz-Rojas, J. Fernández-Rossier, and J. J. Palacios, *Phys. Rev. Lett.* **102**, 136810 (2009).
- ¹⁰W. Y. Kim and K. S. Kim, *Nat. Nanotechnol.* **3**, 408 (2008).
- ¹¹D. Gunlycke, D. A. Areshkin, J. Li, J. W. Mintmire, and C. T. White, *Nano Lett.* **7**, 3608 (2007).
- ¹²K. Harigaya and T. Enoki, *Chem. Phys. Lett.* **351**, 128 (2002).
- ¹³J. Fernández-Rossier and J. J. Palacios, *Phys. Rev. Lett.* **99**, 177204 (2007).
- ¹⁴W. L. Wang, O. V. Yazyev, S. Meng, and E. Kaxiras, *Phys. Rev. Lett.* **102**, 157201 (2009).
- ¹⁵M. Ezawa, *Phys. Rev. B* **77**, 155411 (2008).
- ¹⁶P. Koskinen, S. Malola, and H. Häkkinen, *Phys. Rev. Lett.* **101**, 115502 (2008).
- ¹⁷T. Wassmann, A. P. Seitsonen, A. M. Saitta, M. Lazzeri, and F. Mauri, *Phys. Rev. Lett.* **101**, 096402 (2008).
- ¹⁸A. Chuvilin, J. C. Meyer, G. Algara-Siller, and U. Kaiser, *New J. Phys.* **11**, 083019 (2009).
- ¹⁹D. C. Elias *et al.*, *Science* **323**, 610 (2009).
- ²⁰O. V. Yazyev and L. Helm, *Phys. Rev. B* **75**, 125408 (2007).
- ²¹L. Brey, H. A. Fertig, and S. Das Sarma, *Phys. Rev. Lett.* **99**, 116802 (2007).
- ²²S. Casolo, O. M. Løvvik, R. Martinazzo, and G. F. Tantardini, *J. Chem. Phys.* **130**, 054704 (2009).
- ²³V. R. Saunders, R. Dovesi, C. Roetti, R. Orlando, C. M. Zicovich-Wilson, N. M. Harrison, K. Doll, B. Civalleri, I. J. Bush, and P. D'arco, Release 1.0.2, Theoretical Chemistry Group, Università Di Torino, Torino (Italy).
- ²⁴J. Fernández-Rossier, *Phys. Rev. B* **77**, 075430 (2008).
- ²⁵E. H. Lieb, *Phys. Rev. Lett.* **62**, 1201 (1989).
- ²⁶J. J. Palacios, D. Jacob, A. J. Pérez-Jiménez, E. S. Fabián, E. Louis, and J. A. Vergés, ALACANT *ab initio* quantum transport package, Condensed Matter Theory Group, Universidad de Alicante, <http://alacant.dfa.ua.es>
- ²⁷J. J. Palacios, J. Fernández-Rossier, and L. Brey, *Phys. Rev. B* **77**, 195428 (2008).
- ²⁸D. Boukhvalov and M. Katsnelson, *Nano Lett.* **8**, 4373 (2008).
- ²⁹J. Lin, J. J. Rhyne, J. K. Furdyna, and T. M. Giebutoicz, *J. Appl. Phys.* **83**, 6554 (1998).
- ³⁰Y.-W. Son, M. L. Cohen, and S. G. Louie, *Phys. Rev. Lett.* **97**, 216803 (2006).
- ³¹D. V. Kosynkin, A. L. Higginbotham, A. Sinitskii, J. R. Lomeda, A. Dimiev, B. K. Price, and J. M. Tour, *Nature (London)* **458**, 872 (2009).
- ³²H. Santos, L. Chico, and L. Brey, *Phys. Rev. Lett.* **103**, 086801 (2009).
- ³³A. Javey, J. Guo, D. B. Farmer, Q. Wang, D. Wang, R. G. Gordon, M. Lundstrom, and H. Dai, *Nano Lett.* **4**, 447 (2004).
- ³⁴C. P. Herrero and R. Ramirez, *Phys. Rev. B* **79**, 115429 (2009).